https://doi.org/10.1016/j.ijepes.2020.105975

An Optimal Modal Coordination Strategy based on Modal Superposition Theory to Mitigate Low Frequency Oscillation in FCWG Penetrated Power Systems

Jianqiang Luo, Siqi Bu, and Fei Teng

***Abstract*—Full converter-based wind power generation (FCWG, e.g. permanent magnet synchronous generator (PMSG)) becomes prevalent in power electronics dominated multi-machine power system (MMPS). With flexibly modified FCWG oscillation modes (FOMs), FCWG has the potential to actuate conducive dynamic interactions with electromechanical oscillation modes (EOMs) of MMPS. In this paper, a mathematical model of FCWG and MMPS is firstly derived to examine the dynamic interactions. Then a novel modal superposition theory is proposed to classify the modal interactions between FOMs and EOMs in the complex plane for the first time. The modal coupling mechanism is graphically visualized to investigate the dynamic interactions, and the eigenvalue shift index is proposed to quantify the dynamic interaction impact on critical EOM. Based on different manifestos in modal coupling mechanism and eigenvalue shift index, a novel methodology to optimize the dynamic interactions between the FCWG and MMPS is designed within the existing control frame. The optimized dynamic interactions (i.e. modal counteraction) can significantly enhance the LFO stability of MMPS, effectiveness of which is verified by both modal analysis and time domain simulations.**

***Index Terms*— Electromechanical oscillation mode (EOM), low frequency oscillation (LFO), permanent magnet synchronous generator (PMSG), modal superposition, optimized interaction.**

I. INTRODUCTION

POWER system low frequency oscillation (LFO) stability could be significantly impacted by the increasing penetration level of wind power generation [1-5]. Full converter-based wind power generation (FCWG, i.e., permanent magnet synchronous generator (PMSG)) is very promising to replace other types of wind power generation (such as doubly-fed induction generator (DFIG)) in the future market owing to the rapid development of power electronics [6-8]. Due to the completely different physical structure of the wind power generators from the conventional thermal power synchronous generators (CSGs), the high penetration of FCWG, especially the replacement of CSGs with FCWG, may lead to inertia and damping reduction of the multi-machine power system (MMPS). In addition, the traditional LFO suppressing measures such as power system stabilizer (PSS) can no longer be applied. New solutions to provide damping functions with FCWG and improve LFO stability need to be investigated.

To assess the integration of wind power generation, the mechanism of how wind power generation interacts with power system needs to be studied. As stated in reference [9], the impact of grid-connected wind farms on the power system are mainly in two folds: i.e. the change of power flow and the dynamic interactions. With the benefit of wind power generation from FCWG to meet the demand of load centers being fully utilized, the dynamic interactions introduced by the integration of FCWG should also be explored to benefit the LFO stability of power systems.

Various control strategies are implemented, and the associated damping controllers are designed to improve the dual dynamic interactions as well as enhance the damping of the power system. Reference [10] offers a cascading control scheme to provide inertia support to the power system via simultaneous utilization of dc-link capacitor energy and wind turbine rotor kinetic energy. A virtual inertia control scheme based on optimized power point tracking (OPPT) controller for PMSG-based wind turbine is proposed to provide inertial response and damping for power system oscillations [11]. The virtual synchronous generator (VSG) control strategy is widely employed to increase the effective inertia and damping of PMSG in [12]. It is reported in [13] that delay of frequency signal and gains of inertia control loop can influence the duration of the peak inertia response, and an over 10s inertia response can be achieved to improve the oscillation stability with the coordination of individual turbines.

However, on the one hand, most control strategies and schemes require auxiliary control devices to realize the damping enhancement, which may increase the complexity of the wind power generation. On the other hand, careful tuning and coordination with other components of the FCWG are needed. This may also add burden to the operation and weaken the robustness of the power system. In this paper, a novel methodology to directly coordinate and improve the dynamic interactions between FCWG and MMPS is proposed. The objective of damping LFOs can be achieved by optimizing the dynamic interactions within the existing conventional control frame.

Therefore, the contributions of this paper are summarized as follows: 1) **Modal superposition theory**: The modal superposition theory is proposed to categorize and analyze all the possible dynamic interactions between FCWG and MMPS. 2) **Modal coupling visualization**: Three categories of modal coupling are extensively elaborated and visualized in the complex plane, which provides theoretical foundation for damping enhancement with proper modal coordination.; 3) **Modal coupling mechanism**: The modal coupling mechanism

is conducted through to explore the modal interactions between FOM and EOM considering the relative locations; 4) **Optimization methodology**: Based on modal superposition theory and eigenvalue shift index, an optimization methodology to optimize the dynamic interactions is proposed to achieve modal counteractions and enhance the overall LFO stability.

The remaining of this paper is organized as follows. Section II presents the system under investigation where an FCWG-based wind farm is connected to a benchmark MMPS. The mathematical model is established, with the FCWG wind farm being modeled as a PMSG controller of MMPS. Section III introduces the modal superposition theory that classifies the modal interactions between FCWG and MMPS. Three categories of modal coupling are analyzed and visualized, and their impact on damping is discussed. Section IV presents the eigenvalue shift index to evaluate the qualitative and quantitative impact of FCWG on LFO stability. Then a novel optimization methodology is proposed to optimize the dynamic interactions as well as realize the optimal modal coordination between FCWG and MMPS. Section V presents a thorough case study to verify the effectiveness of the proposed method. Analyses in both complex domain and time domain are performed. Section VI concludes the paper.

II. MATHEMATICAL MODEL

Fig. 1 shows that an FCWG-based wind farm is connected to MMPS at the common coupling point (PCC). The FCWG-based wind farm is modeled as a PMSG with full converters. The collective behavior of a group of wind turbines in the wind farm can be presented by an equivalent lumped machine as demonstrated in previous studies [14-16]. In this paper, introduction and discussion are presented for an equivalent PMSG connected to the MMPS so as to facilitate the analyses.

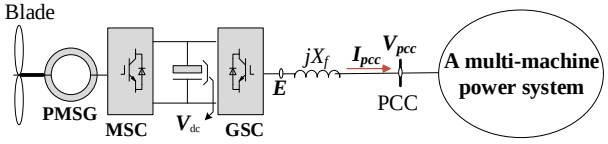

Fig.1. Physical configuration of an FCWG connected to a multi-machine power system.

The integration of FCWG consists of four main parts: 1) The PMSG; 2) The machine side converter (MSC) and the associated control system; 3) The DC-link, the grid side converter (GSC) and the associated control system; 4) The synchronous reference frame phase locked loop (SRF-PLL) which keeps the synchronization with MMPS.

In the derivation of mathematical model, a detailed 13th-order dynamic model of PMSG, the associated converters and control systems is used [17]. In addition, a second-order SRF-PLL is used [18]. In total, the 15the order mathematical model of FCWG can be expressed as

$$\begin{cases} \dfrac{d}{dt}\Delta \boldsymbol{X}_{pp} = \boldsymbol{A}_{gp}\Delta \boldsymbol{X}_{pp} + \boldsymbol{B}_{gp}\Delta \boldsymbol{V}_{pcc} \\ \Delta \boldsymbol{I}_{pcc} = \boldsymbol{C}_{gp}\Delta \boldsymbol{X}_{pp} + \boldsymbol{D}_{gp}\Delta \boldsymbol{V}_{pcc} \end{cases} \tag{1}$$

where $\Delta X_{pp} = [\,\Delta\psi_{psd}\ \Delta\psi_{psq}\ \Delta\omega_{pr}\ \Delta x_{p1}\ \Delta x_{p2}\ \Delta x_{p3}\ \Delta I_{pcd}\ \Delta I_{pcq}\ \Delta V_{pdc}\ \Delta x_{p4}\ \Delta x_{p5}\ \Delta x_{p6}\ \Delta x_{p7}\ \Delta x_{pll}\ \Delta\theta_{pll}\,]$, the 1st ~3rd state variables denote the dynamics of PMSG wind turbine, the 4th~6th state variables denote the dynamics of MSC, the 7th~8th state variables denote the dynamics of the filter, the 9th~10th state variables denote the dynamics of DC capacitor, the 11th~13th state variables denote the dynamics of GSC, and the 14th~15th state variables denote the dynamics of SRF-PLL. $\Delta \boldsymbol{V}_{pcc}=[\Delta V_x \quad \Delta V_y]^T$ is the voltage variation of PCC and $\Delta \boldsymbol{I}_{pcc}=[\Delta I_x \quad \Delta I_y]^T$ is current injection variation from PMSG at PCC under the common x-y coordinate system. $\boldsymbol{A_{gp}}$, $\boldsymbol{B_{gp}}$, $\boldsymbol{C_{gp}}$, $\boldsymbol{D_{gp}}$ denote the state space matrices of FCWG.

Meanwhile, the state space equations of MMPS can be derived as [19]

$$\begin{cases} \dfrac{d}{dt}\Delta \boldsymbol{X}_{g} = \boldsymbol{A}_{gT}\Delta \boldsymbol{X}_{g} + \boldsymbol{B}_{gT}\Delta \boldsymbol{I}_{pcc} \\ \Delta \boldsymbol{V}_{pcc} = \boldsymbol{C}_{gT}\Delta \boldsymbol{X}_{g} + \boldsymbol{d}_{I}\Delta \boldsymbol{I}_{pcc} \end{cases} \tag{2}$$

where $\Delta \boldsymbol{X_g}$ denotes the vector of all the state variables of the CSGs. $\boldsymbol{A_{gT}}$, $\boldsymbol{B_{gT}}$, $\boldsymbol{C_{gT}}$, $\boldsymbol{d_I}$ denote the state space matrices of MMPS.

Hence, by combining (1) and (2), the linearized closed-loop interconnected model of the entire power system is obtained as

$$\frac{d}{dt}\begin{bmatrix} \Delta \mathbf{X_g} \\ \Delta \mathbf{X_{pp}} \end{bmatrix} = \begin{bmatrix} \mathbf{A_{gT}} & \mathbf{B_{gT}}C_{gp} \\ B_{gp}\mathbf{C_{gT}} & A_{gp} + B_{gp}d_I C_{gp} \end{bmatrix}\begin{bmatrix} \Delta \mathbf{X_g} \\ \Delta \mathbf{X_{pp}} \end{bmatrix} \tag{3}$$

In Fig.1, the FCWG acts as a current source $\boldsymbol{I}_{pcc} = \boldsymbol{I}_{pcc0} + \Delta \boldsymbol{I}_{pcc}$, which provides the grid supporting function [20] for the power system and responses to the variation of PCC voltage $\boldsymbol{V}_{pcc} = \boldsymbol{V}_{pcc0} + \Delta \boldsymbol{V}_{pcc}$, where the subscript '0' denotes the steady-state value of the corresponding variable and 'Δ' denotes the variation of the corresponding variable at some equilibrium operating points. Under steady state, the feedback signal $\Delta \boldsymbol{V}_{pcc} = 0$ and output $\Delta \boldsymbol{I}_{pcc} = 0$, the FCWG wind farm acts as a constant power source with a constant current injection $\boldsymbol{I}_{pcc0}$, which only influences the power flow. However, once disturbances happen in the power system, voltage fluctuations at PCC will be introduced into FCWG and its associated control systems will respond to MMPS in the form of current variation. Hence, the FCWG can influence the dynamic performance of the power system and in some degree act as a sort of controller from the point of view of MMPS.

To study the dynamic interactions from FCWG, a linearized model is shown in Fig. 2, where the FCWG is mathematically modeled as a controller of MMPS, which denotes as the '**PMSG controller**' as a matter of convenience in the rest of this paper. The voltage variation $\Delta \boldsymbol{V}_{pcc}=[\Delta V_x \quad \Delta V_y]^T$ at the point of common coupling (PCC) acts as the feedback signal and the output is the current variation injection $\Delta \boldsymbol{I}_{pcc}=[\Delta I_x \quad \Delta I_y]^T$ that influences the dynamic performance of the MMPS. According to the power flow information at PCC, the transfer functions of both MMPS and the PMSG controller can be derived as $\boldsymbol{G}(s)$ and $\boldsymbol{H}(s)$, respectively. The formation of the transfer functions can be

obtained from the state space matrices derived above.

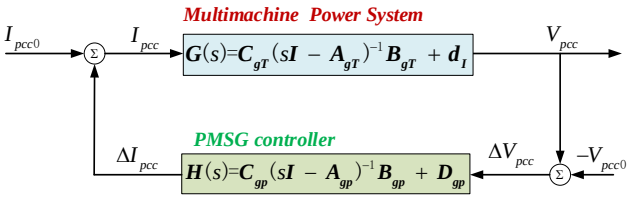

Fig. 2. Mathematical model of a PMSG controller connected to the multi-machine power system.

Due to the AC-DC-AC configuration, FCWG is decoupled from MMPS and do not normally respond to the dynamics change of the main grid. Moreover, the wind farm owners normally adopt conservative control strategies which mainly focus on the improvement of the dynamic performance of the wind turbines themselves rather than respond actively to the disturbances of MMPS. Therefore, the dynamic interactions between FCWG and MMPS are usually weak and even negative (e.g. modal resonance conditions).

However, through properly tuning the controllers of grid side converter (GSC), considerable dynamic interactions with MMPS are achievable for the benefit of oscillation stability. With a careful investigation on the LFO characteristic of MMPS, it is feasible to control the participation of FCWG in LFOs to improve the dynamic interactions and thus oscillation stability. As a result, the positive contributions from FCWG towards MMPS can be obtained.

III. Modal Superposition Theory

A. Modal Superposition Classification

The integration of FCWG introduces new FCWG oscillation modes (FOMs) to MMPS. The FOMs may interact with the open-loop electromechanical modes (EOMs) of MMPS. The dynamic modal interaction process can be designated as **modal superposition**. Fig. 3 illustrates all the classifications of modal superposition between FCWG and MMPS and the impact on system damping.

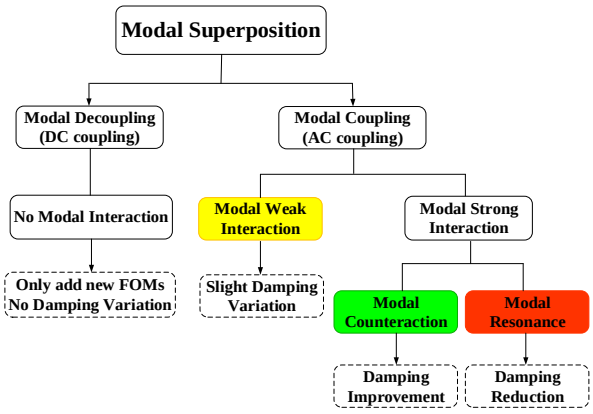

Fig. 3 Classification of modal superposition.

A.1 Modal Decoupling (DC coupling)

The integration of FCWG not only provides power injections, but also induces dynamic interactions with MMPS. Due to the full-scale converters and corresponding control strategy, not all the FOMs participate in the modal interactions. Some of FOMs (e.g. the oscillation modes related to PMSG wind turbine and machine side converter (MSC)) are connected at the point of DC coupling (i.e. the DC capacitor) and thus decoupled from MMPS. This kind of modal superposition is called **modal decoupling**, which only introduces new modes to the entire power system and does not interact with the original modes of MMPS.

Therefore, the new oscillation modes are all independent FOMs, their characteristics are determined by its physical parameters and operating points, while the original modes of MMPS remain the same. As a result, the damping of critical EOM of MMPS is not affected.

A.2 Modal Coupling (AC Coupling)

The rest of FCWG is usually connected to MMPS via the point of AC coupling (i.e. PCC), and the associated control system at the grid side converter (GSC) normally responses to the PCC voltage variation from MMPS. Therefore, the FOMs that relate with DC link, GSC and phase-locked loop (PLL) will interact with the EOMs of MMPS. This type of modal interaction is named as **modal coupling**. Based on the coupling strength and characteristics, they can be classified in three main categories of modal coupling.

First, based on the coupling strength, the modal coupling can be divided into weak interaction and strong interaction. If the modal coupling is strong enough to influence the critical EOM considerably, such as reduces the damping ratio noticeably or even leads to negative damping ratio and instability, it is defined as **modal strong interaction**. Otherwise, it is called **modal weak interaction (Yellow)**. Normally, the dynamic interactions between FCWG and MMPS are very weak. The FOMs are mainly determined by the physical parameters and related control strategies that are commonly designed to focus on its own dynamic performance. Therefore, the impact of FCWG is to generate a weak interaction that superposes on the critical EOM and sometimes can be negligible.

The strong interactions between FCWG and MMPS may be detrimental or beneficial. If the strong modal interactions deteriorate the damping ratio of the critical EOM and threat LFO stability, it is called **modal resonance (Red)**. Under modal resonance, the newly introduced FOM resonates with the original EOM, and EOM tends to move towards right half complex plane, which magnifies the electromechanical oscillation and jeopardizes the LFO stability. On the contrary, if the interaction between FOM and EOM has a positive effect on the damping ratio of EOM, it is called **modal counteraction (Green)**. In this case, one of FOMs significantly interacts with the critical EOM and pulls the EOM towards the left of the complex plane. As a result, the system damping is improved as well as the LFO stability.

The modal superposition between FOM and EOM can conspicuously influence the LFO stability once modal strong interaction is induced. In normal weak interaction condition, the FOMs usually have different oscillation frequency from

critical EOM, which are well damped due to its well-tuned control parameters. However, under some circumstance, if the oscillation frequency of FOM is close to the frequency of EOM, the strong modal interactions (modal resonance or modal counteraction) may much likely happen, which result in either considerable damping reduction or improvement. Therefore, appropriate modal coordination between FOM and EOM should be paid attention to circumventing modal resonance and achieving modal counteraction.

B. Modal Coupling Classification Visualization

In practice, if the damping ratio of critical EOM is larger than 5%, the power system is identified to be a strong system that has enough damping margin to ensure LFO stability. However, if the damping ratio of critical EOM is less than 5% or even 3%, the system is identified to be weak [19]. Under such circumstance, the dynamic interactions from FCWG may become eminent or even crucial for LFO stability. In this paper, the core concern is to assess the dynamic interactions between FCWG and a weak MMPS and propose a modal coordination strategy to enhance LFO stability.

For a weak MMPS, the open-loop critical EOM usually locates at the right of 5% damping ratio line and almost stays at the same place or nearby in most operating points, whereas the open-loop FOM can be flexibly relocated within acceptable range. The modal couplings also vary with different locations between open-loop FOM and open-loop EOM. Fig. 4 illustrates the modal coupling classification visualization between FCWG and MMPS for a fixed open-loop critical EOM and a varying open-loop FOM. If the open-loop FOM locates in the yellow area, the modal interactions are quite weak, and do not impose significant impact on LFO stability and can be neglected in most cases. If the open-loop FOM locates in the green area, strong modal counteraction may happen that pulls the critical EOM towards the left and meliorates the system damping.

If the open-loop FOM locates in the red area, strong modal resonance may happen that resists and pushes the critical EOM towards the right of complex plane or even leads to instability.

For the entire closed-loop system, the eigenvalues related with open-loop FOM and open-loop EOM shift in the complex plane due to modal interactions as reflected in Fig. 6. Fig. 6(a) depicts the typical eigenvalue movements of critical EOM and FOM under weak interaction, while Fig. 6(b) and Fig. 6(c) demonstrate that of modal counteraction and modal resonance under strong interaction respectively.

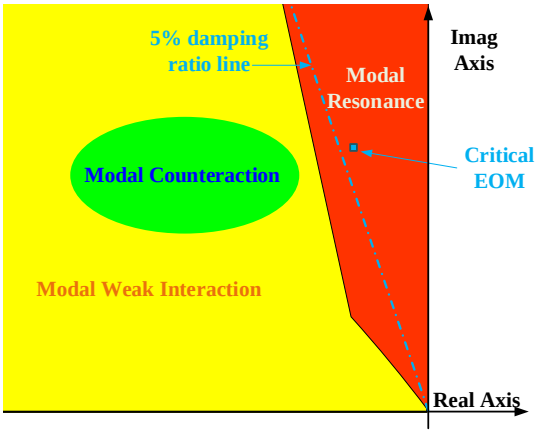

Fig. 4 Diagram of modal coupling classification based on a fixed open-loop critical EOM.

C. Modal Coupling Classification Mechanism

To verify the modal coupling classification, a small test system is established as shown in Fig. 5. The critical open-loop EOM can be calculated from the generator transfer function G(s), while the open-loop FOM is solved from the controller transfer function H(s).

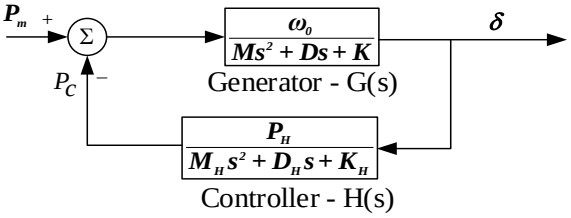

Fig. 5 The configuration of the sample system.

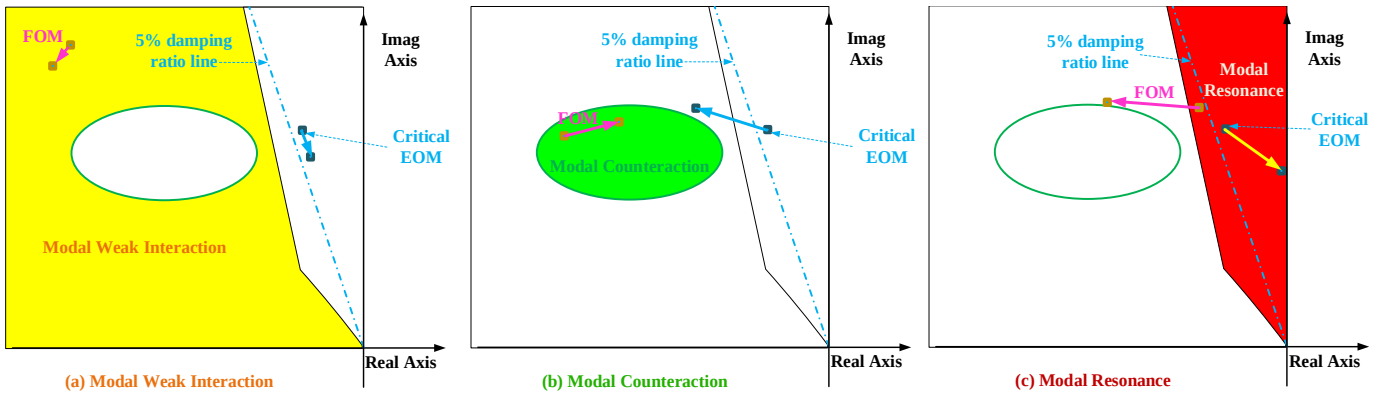

Fig. 6 Eigenvalue shifts of critical EOM and FOM under different categories of modal coupling.

For a fixed open-loop EOM, the upper left half complex plane can be classified into different areas with respect to the location of open-loop FOM while considering different modal interactions, as illustrated in Fig. 7 and Fig. 8. To perform the area classification, we enumerate the most possible area in left half complex plane. Since there are infinite locations in the selected area, we set up a rule to examine 50,000 locations of FOM (area search range: real part range: -5 ~ 0, step length: 0.01, imaginary part range: 0 ~ 10, step length: 0.1) for each subfigure. For every FOM location, closed-loop eigenvalue analysis is implemented, and its impact on closed-loop EOM damping is analyzed. Based on the damping performance with respect to different modal coupling conditions, the FOM location is colored.

As demonstrated in Fig. 7 and Fig. 8, the yellow area denotes the modal weak interactions, green area implies the modal counteractions, while the blue, red and black areas reflect the modal resonances (ordinary modal resonance, strong resonance and instability, respectively). For a fixed open-loop EOM, the location of FOM influences the overall oscillation stability. A magenta point of FOM indicates the optimal location of FOM so that the entire closed-loop system has the largest damping ratio. Based on analyses above, several findings are concluded as follows:

1) For a specific system, the integration of controller introduces new modes (e.g. FOM) that may interact with the original mode (i.e. the open-loop EOM). With different locations of open-loop EOM, the area classifications of open-loop FOM also vary in the complex plane.
2) Improper locations of open-loop FOM may induce modal resonance that exasperates the system damping or even leads to instability (e.g. red and black areas).
3) For a fixed oscillation frequency open-loop EOM, the smaller the damping ratio is, the larger the green area is (Fig. 7), which indicates that modal counteractions are easier to be achieved and more effective in a weak system. The damping improvement in a strong system is quite limited.
4) For a fixed damping ratio open-loop EOM, the lower the oscillation frequency is, the larger the green area is (Fig. 8), which implies that the LFO modes are more sensitive in the modal interactions, and modal counteractions are more promising in depressing LFOs.
5) The optimal open-loop FOM usually has almost the same frequency as the open-loop EOM and locates at the left but not very far away, which is an important characteristic in narrowing the search range of optimal control parameters.

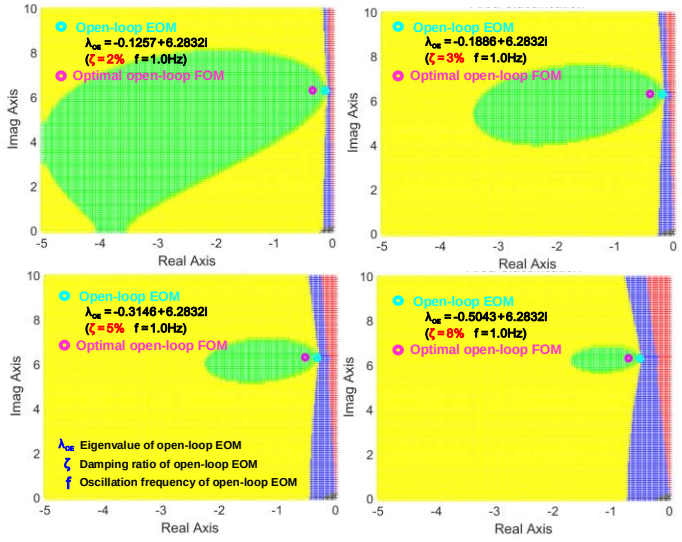

Fig. 7 Area classification considering different damping ratios of open-loop EOM.

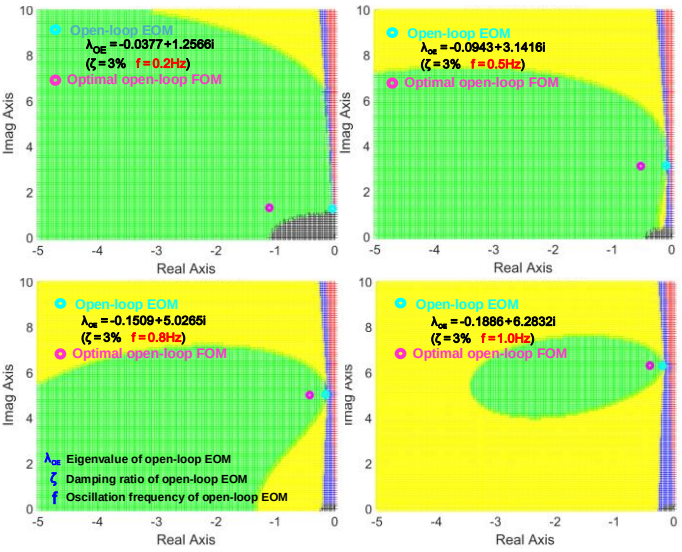

Fig. 8 Area classification considering different oscillation frequencies of open-loop EOM.

IV. Eigenvalue Shift Index and Optimal Modal Coordination Strategy

In this section, assessments on the impact of the PMSG controller are presented. Eigenvalue shift index is proposed to investigate the dynamic interaction impact on the critical EOM in a quantitative manner and provide a clear understanding of how FCWG influences the LFO stability of MMPS. On this basis, the modal coordination optimization is proposed to realize modal counteraction between FOM and critical EOM and enhance the damping of MMPS.

A. Eigenvalue Shift Index

Assume $\lambda_i=-\sigma_i+j\omega_i$ and $\boldsymbol{v}_i$, $i=1,2,...M$ as the ith eigenvalue and associated right eigenvectors of the state matrix $\boldsymbol{A_{gT}}$ of MMPS. Denote $\lambda_i=-\sigma_i+j\omega_i$ as the eigenvalue of the ith

oscillation mode of MMPS excluding the dynamic interactions of the PMSG controller (i.e. $\Delta \boldsymbol{I}_{pcc}=[\Delta I_x \quad \Delta I_y]^T = \boldsymbol{0}$) , and $\hat{\lambda}_i=-\hat{\sigma}_i+j\hat{\omega}_i$ is the eigenvalue of the ith oscillation mode including the dynamic interactions of PMSG controller (i.e. $\Delta \boldsymbol{I}_{pcc}=[\Delta I_x \quad \Delta I_y]^T \neq \boldsymbol{0}$). Both λ_i and $\hat{\lambda}_i$ can be obtained through eigenvalue analyses on the open-loop system and closed-loop system respectively. Therefore, the impact of dynamic interactions of the PMSG controller can be mathematically defined by the eigenvalue shift index (ESI) by the equation: ESI=$\Delta\lambda_i=\hat{\lambda}_i-\lambda_i$.

The real part of ESI (denoted as Re(ESI)) is related to the damping of the power system. If Re(ESI)<0, it means the dynamic interactions introduce extra damping, and hence the integration of the PMSG controller is beneficial for the power system oscillation stability. On the other hand, if Re(ESI)>0, it means the dynamic interactions deteriorate the system damping, and hence the integration of the PMSG controller is detrimental for the power system oscillation stability.

Based on analyses in section III, the modal counteractions can benefit the damping MMPS. To realize modal counteractions, the proper modal coordination on the PMSG controller is needed. To deeply dig this potential to enhance the LFO stability, damping torque analysis is employed to quantify the impact mathematically.

The rearrangement of state space matrix $\boldsymbol{A}_{gT}$, $\boldsymbol{B}_{gT}$,$\boldsymbol{C}_{gT}$, $\boldsymbol{d}_I$ of MMPS can be performed as

$$\begin{aligned} \frac{d}{dt}\begin{bmatrix}\Delta\boldsymbol{\delta}\\ \Delta\boldsymbol{\omega}\\ \Delta\boldsymbol{z}\end{bmatrix} &= \begin{bmatrix}\boldsymbol{0} & \boldsymbol{\omega}_0\boldsymbol{I} & \boldsymbol{0}\\ \boldsymbol{A}_{21} & \boldsymbol{A}_{22} & \boldsymbol{A}_{23}\\ \boldsymbol{A}_{31} & \boldsymbol{A}_{32} & \boldsymbol{A}_{33}\end{bmatrix}\begin{bmatrix}\Delta\boldsymbol{\delta}\\ \Delta\boldsymbol{\omega}\\ \Delta\boldsymbol{z}\end{bmatrix} + \begin{bmatrix}\boldsymbol{0}\\ \boldsymbol{b}_{I2}\\ \boldsymbol{b}_{I3}\end{bmatrix}\Delta\boldsymbol{I}_{pcc} \\ \Delta\boldsymbol{V}_{pcc} &= \begin{bmatrix}\boldsymbol{C}_{g1} & \boldsymbol{C}_{g2} & \boldsymbol{C}_{g3}\end{bmatrix}\begin{bmatrix}\Delta\boldsymbol{\delta}\\ \Delta\boldsymbol{\omega}\\ \Delta\boldsymbol{z}\end{bmatrix} + \boldsymbol{d}_I\Delta\boldsymbol{I}_{pcc} \end{aligned} \tag{4}$$

A detailed diagram to quantify the contribution from the PMSG controller to EOM eigenvalue shifts is shown in the detailed diagram is shown in Fig. 9. It is worth mentioning that if we further rearrange the structure of (4), other oscillation modes (e.g. sub-synchronous oscillation modes) can also be evaluated.

The forward path (as highlighted in blue) from the PMSG controller to electromechanical oscillation loop of MMPS is [21]

$$\frac{\Delta\boldsymbol{T}}{\Delta\boldsymbol{I}_{pcc}} = \boldsymbol{F}(s) = \boldsymbol{b}_{I2} + \boldsymbol{A}_{23}(s\boldsymbol{I} - \boldsymbol{A}_{33})^{-1}\boldsymbol{b}_{I3} \tag{5}$$

By employing damping torque analysis in [22], the eigenvalue shift of ith eigenvalue λ_i (ith EOM) of MMPS caused by the integration of PMSG controller can be calculated as

$$\Delta\lambda_i = \sum_{k=1}^{n} S_{ik}\boldsymbol{F}(\lambda_i)\boldsymbol{H}(\lambda_i)\gamma_{ik}(\lambda_i) \tag{6}$$

where S_{ik} is the sensitivity of λ_i with respect to the damping torque coefficient of the kth SG in MMPS, $\boldsymbol{H}$ is the transfer function of the PMSG controller, γ_{ik} is the relationship between $\Delta\boldsymbol{V}_{pcc}$ and $\Delta\omega_k$.

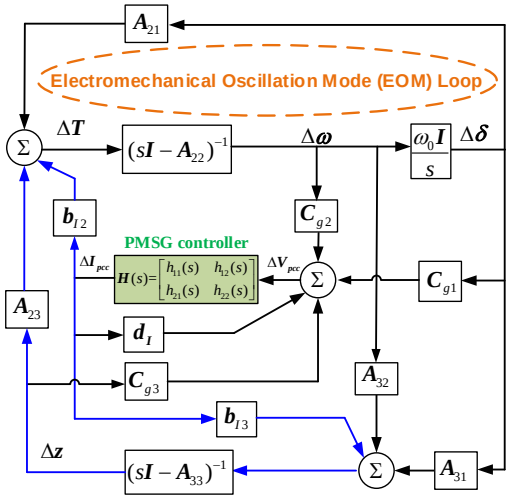

Fig. 9 Contribution from PMSG controller to the EOM of MMPS.

From (6), it can be seen that the eigenvalue shift of the EOM of MMPS is closely related to the transfer function $\boldsymbol{H}(s)$ of the PMSG controller. Since $\boldsymbol{H}(s)$ is mainly determined by the parameters of the PMSG and its associated control system, if λ_i is close to the FOMs, $\boldsymbol{H}(\lambda_i)$ may become very large that leads to considerable ESI. With proper tuning and optimization of the PMSG controller, it is possible to obtain an eigenvalue shift which has a negative real part, which turns out to move the eigenvalue of the EOM towards the left in the complex plane. The objective of PMSG controller parameter tuning is to realize a modal coordination with the critical EOM so that the modal counteractions happen and improve the system damping.

B. Modal Coordination Optimization

By optimizing the controller parameters, the FOMs can be relocated to induce strong modal counteractions with the critical EOM and thus enhance the LFO stability of MMPS. Based on the modal superposition theory proposed in Section III, the possible FOM range to achieve the modal counteraction can be defined in the complex plane and hence narrow the search range of optimal parameters and facilitate the modal coordination optimization. The tuning process can therefore be defined as an optimization problem to obtain the largest negative part of the eigenvalue shift in critical EOM.

$$\text{Minimize} \quad Re(ESI) = real(\Delta\lambda_{iEOM}) \tag{7}$$

where $\Delta\lambda_{iEOM}$ is the eigenvalue shift of the critical EOM of MMPS.

The modal coordination optimization is illustrated in Fig. 10.

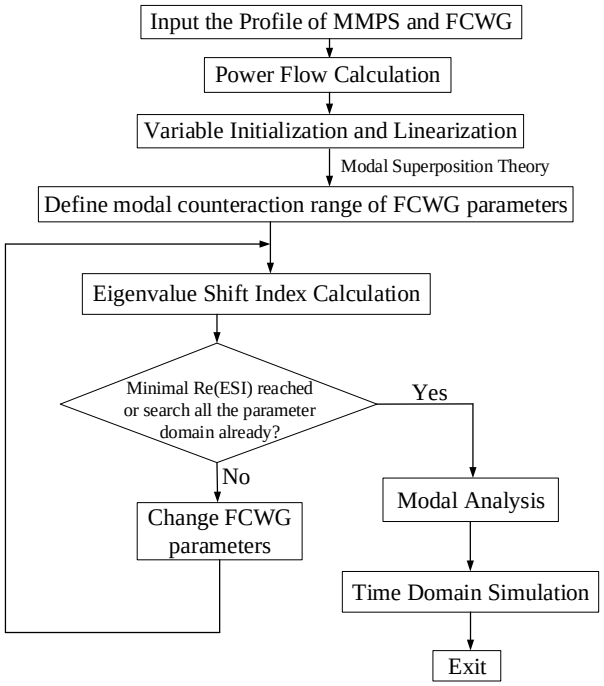

Fig. 10 Flowchart of parameter tuning in the PMSG controller.

To ensure the robustness of the proposed optimization strategy, the optimization is conducted in the worst case scenario, not only for the worst damping conditions of MMPS (e.g. heavy load condition), but also for the worst dynamic interactions from FCWG (i.e. the highest power injection from FCWG and the modal resonance conditions that possess the worst dynamic interactions) as suggested by [9]. With this optimization strategy, the optimized parameters can fully guarantee their robustness when operating condition changes, which has been verified by the following case studies.

It can be also noted that the proposed optimization strategy relies on the availability of the entire system model. However, when the system model is completely or partially unavailable, the optimal modal coordinating strategy can still be implemented by using a measurement-based technique (e.g., using PMU to measure typical LFOs). The important findings based on modal superposition theory are still valid.

V. Case Study

A. Introduction of the Example System

An example power system is presented in Fig. 11 to study the dynamic interactions between FCWG and MMPS. The New England power system is integrated with an FCWG wind farm connected at Bus 22. In the example system, the simplified third-order model of the synchronous generators (SGs) and a first-order of the automatic voltage regulator (AVR) are adopted [23]. No PSS is installed on any SG. The FCWG wind farm is modeled as a PMSG connected to the power system through full converters, the detailed 15th-order model of PMSG is used. The PMSG adopts reactive power control with a fixed power factor (0.95). The typical controller parameters in [24] are used in PMSG.

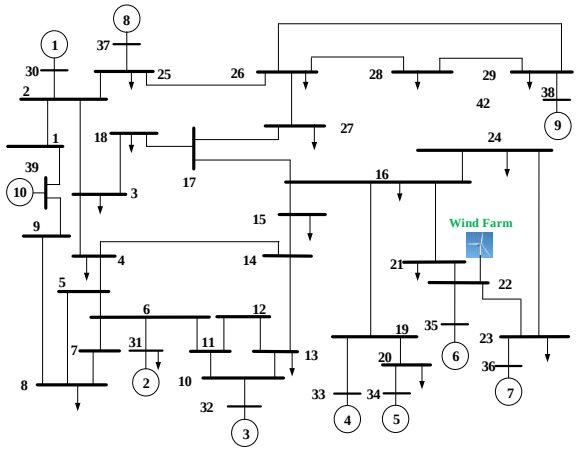

Fig. 11 Configuration of New England power system integrated with an FCWG wind farm.

B. Open-loop MMPS and Initial Condition Setting

To examine the original EOMs of MMPS, the active power injection of the PMSG is first set to be zero (i.e Pw=0 p.u.). Then, the nine low frequency EOMs in the open-loop New England power system are identified by modal analysis, ranging from 0.4Hz ~ 1.3Hz, as shown in Table I.

TABLE I
THE TYPICAL EOMS OF THE NEW ENGLAND POWER SYSTEM

Eigenvalue of EOM	Frequency (Hz)	ELCR*1	Associated SGs
-0.1537 + 3.1235i	**0.4971**	10.16	1,2,3,4,5,6,7,8,9,**10***2
-1.5016 + 4.8621i	0.7738	14.38	3,4,**5**,6,7,9
-0.1886 + 5.2913i	0.8421	18.14	2,3,6,7,**9**
-0.3245 + 5.9365i	0.9448	31.03	**2**,3,6,7
-0.5277 + 6.2109i	0.9885	84.21	**1**,3,6,7,8,9
-0.2641 + 6.6454i	1.0576	46.29	2,**3**
-0.5344 + 7.6212i	1.2129	25.92	**4**,5,6,7,8
-0.4056 + 7.6556i	1.2184	32.04	4,6,**7**
-0.4478 + 7.7884i	1.2396	35.21	1,4,**8**

*1: ELCR means electromechanical loop correlation ratio which classifies the EOMs from other oscillation modes; *2: The number in bold (e.g.**10**) in the last column means the tenth SG possesses the largest participation factor.

By analyzing the participation factors (PFs) with related SGs in each EOM, the local modes and inter-area modes are easily classified [23]. The critical mode is usually the inter-area mode with the lowest oscillation frequency (e.g. 0.4971Hz in Table I) that dominates the LFO stability, and in which almost all the SGs are participated.

C. Modal Analysis on Modal Couplings

As stated in section III, there are three categories of modal coupling. With typical controller parameters in PMSG, the modal interaction between FCWG and MMPS is identified to be **weak interaction** condition above.

By performing the proposed optimization methodology shown in Fig. 10, the controller parameters of FCWG is optimized and optimal modal coordination is achieved. The worst case with a low damping ratio of with 2.31% under modal weak interaction conditions (i.e. Pw=3.5p.u. with original typical controller parameters) is chosen as the base to conduct modal coordination optimization. After optimization, it is designated as the **optimized interaction** condition (i.e. modal counteraction) in this case study.

To demonstrate all the modal coupling conditions between FCWG and MMPS, the strong modal resonance (e.g. the open-loop modal resonance (OLMR) in [25]) is also employed for comparison and gives a deeper insight on the impact of modal interactions. This is designated as **strong resonance** condition (i.e. modal resonance).

As it is known that the operating points of the FCWG and MMPS may vary and have important impacts on oscillation stability. Therefore, to carefully examine three categories of modal coupling, different operation points, i.e. active power injection ranges from 0p.u. to 3.5p.u., are considered and compared through modal analysis. The closed-loop oscillation modes of associated FOM and critical EOM with different operating points are calculated and shown in Table II.

TABLE II
MODAL ANALYSES COMPARISON OF THREE INTERACTION CATEGORIES UNDER DIFFERENT WIND POWER INJECTIONS

Active power of PMSG (p.u.)	Interaction Categories	Modal Weak Interaction	Modal Counteraction via Optimized Interaction	Modal Resonance with OLMR
Pw=0.0	Critical EOM (Damping Ratio)	-0.1537 +3.1235i (4.91%)	-0.1537 +3.1235i (4.91%)	-0.1537 +3.1235i (4.91%)
	FOM (Damping Ratio)	-2.2274 +5.8990i (35.32%)	-0.4166 +2.5617i (16.05%)	-0.1215 +3.2270i (3.76%)
	PF of PMSG	0.00%	0.00%	0.00%
Pw=0.5	Critical EOM (Damping Ratio)	-0.1434 +3.1084i (4.61%)	-0.1620 +3.1313i (5.17%)	-0.0853 +3.0614i (2.79%)
	FOM (Damping Ratio)	-2.2132 + 5.9111i (35.06%)	-0.4051 + 2.5662i (15.59%)	-0.1932 + 3.2782i (5.88%)
	PF of PMSG	0.23%	3.05%	30.58%
Pw=1.5	Critical EOM (Damping Ratio)	-0.1210 +3.0773i (3.93%)	-0.2074 +3.0759i (6.73%)	-0.0344 +2.9740i (1.16%)
	FOM (Damping Ratio)	-2.1836 + 5.9364i (34.52%)	-0.3775 + 2.5762i (14.50%)	-0.2504 + 3.3434i (7.47%)
	PF of PMSG	0.71%	9.71%	35.60%
Pw=2.5	Critical EOM (Damping Ratio)	-0.0964 +3.0446i (3.16%)	-0.2528 +3.0433i (8.28%)	-0.0000 +2.9060i (0.00%)
	FOM (Damping Ratio)	-2.1529 + 5.9635i (33.96%)	-0.3412 + 2.5857i (13.08%)	-0.2904 + 3.3884i (8.54%)
	PF of PMSG	1.19%	17.11%	36.45%
Pw=3.5	Critical EOM (Damping Ratio)	-0.0695 +3.0101i (2.31%)	-0.3086 +3.0150i (10.18%)	0.0288 +2.8454i (**-1.01%**)
	FOM (Damping Ratio)	-2.1215 + 5.9926i (33.37%)	-0.2938 + 2.5898i (11.27%)	-0.3239 + 3.4248i (9.42%)
	PF of PMSG	1.67%	24.89%	36.39%

With the increase of active power injections from FCWG, with the normal weak interaction condition, the dynamic interactions have limited impact on critical EOM, the main impact from FCWG is the power flow changes that possess variation on power flow structure of the power system, which is also confirmed in [18]. As demonstrated by the blue line in Fig.12, the dynamics of FCWG worsen the damping ratio to a moderate degree. However, if strong resonance is involved (as demonstrated by the black line), the damping ratio of critical EOM decreases quickly and leads to instability.

By implementing modal coordination optimization, the dynamic interactions between the FCWG and MMPS can be reversed, i.e. the damping ratio of critical EOM can be raised with increasing active power injection of the PMSG (as denoted by the magenta line) and the eigenvalue loci in Fig. 12 also implies the critical EOM tends to move towards left, and the LFO stability has been enhanced.

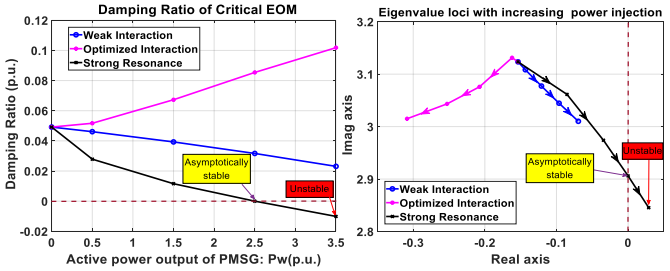

Fig. 12 The impact on critical EOM with increasing active power injection of PMSG.

The closed-loop power system is a multi-input-multi-output (MIMO) system, the singular value response of the power system is illustrated in Fig. 13 to assess the frequency domain response. It can be performed by Matlab coding [26]. As the low frequency domain is our main concern, to make a clear sight, only 0.2Hz ~2.0 Hz (1.26rad/s ~12.57rad/s) is drawn in Fig. 13 with the PMSG power injection Pw=1.5p.u.

Strong resonance condition has the highest peak at the frequency 2.97rad/s with 0.882dB while in the optimized interaction condition, the critical oscillation peak at the frequency 3.07rad/s is the lowest with -10.1dB that indicates the critical EOM is well damped. This is also perfectly matched with the modal analysis results in Table II. At the same time, it can be found that other local EOMs can also be compared (as displayed by the red doted circle), and the optimized interaction condition also has lower peaks in other EOMs in a rough estimation. This finding indirectly proves that optimized interactions do not deteriorate other EOMs of MMPS.

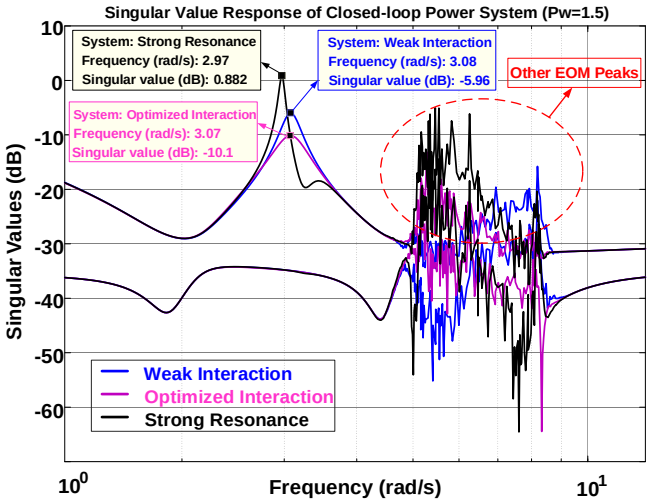

Fig. 13 Singular value response of the closed-loop power system when the active power injection of PMSG Pw=1.5p.u.

The PMSG participation level in critical EOM is also examined in Fig. 14. It is noteworthy that the power injection may play as a quasi-amplifier that magnifies the dynamic interactions although it is not strictly linear, as shown in Fig. 14(a) and Fig. 14(b).

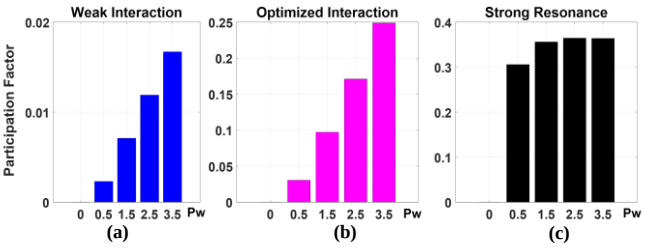

Fig. 14 Comparison of the PMSG participation in critical EOM under different modal couplings.

Under normal weak interaction condition, the participation factor of PMSG grows with the increasing active power injection but remains at a very low level (PF<0.018). With optimized interaction, the participation factor of PMSG increases with a considerable degree (PF=0.25 when Pw=3.5), which significantly influences the critical EOM. For the strong resonance condition, the participation factors are much higher, and the critical EOM is almost dominated by the PMSG controller. Hence, its impact on LFO stability is huge and may lead to remarkable decrease in damping and even leads to instability (as also shown in Fig. 12).

D. Time Domain Simulation Verification

Since the optimized interaction is usually based on the extreme case (usually low damping operation conditions), the optimized interaction of FCWG can possess positive mitigation effect on LFO stability when the operation condition varies.

To further confirm the effectiveness of optimization, the dynamic performances of the test system under small disturbance and large disturbance conditions are examined via time domain simulations respectively.

D.1 Small Disturbance Response

The simulation condition is set to be: at t=0.2s, a **5% step increase of mechanical power reference** occurs at SG1 and subsequently drops to original after 100ms. Three categories of dynamic interactions with different power injections (Pw increases from 1.5 p.u. ~ 3.5 p.u.) are investigated. Due to the limitation of space, only the terminal bus voltage and active power output of SG10 and PMSG are compared, as shown in Fig. 15~Fig. 17.

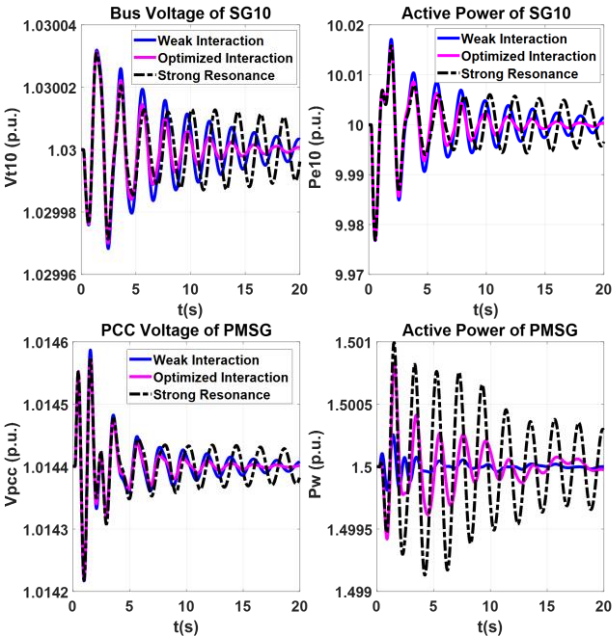

Fig. 15 Small disturbance dynamics comparison: Pw=1.5p.u.

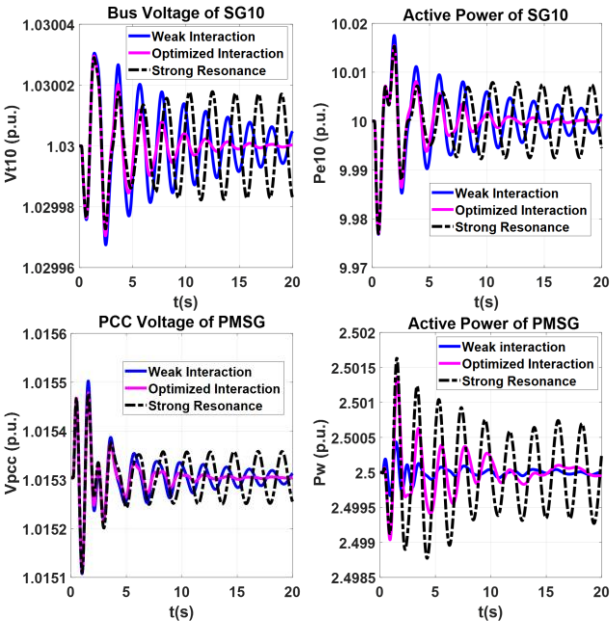

Fig. 16 Small disturbance dynamics comparison: Pw=2.5p.u.

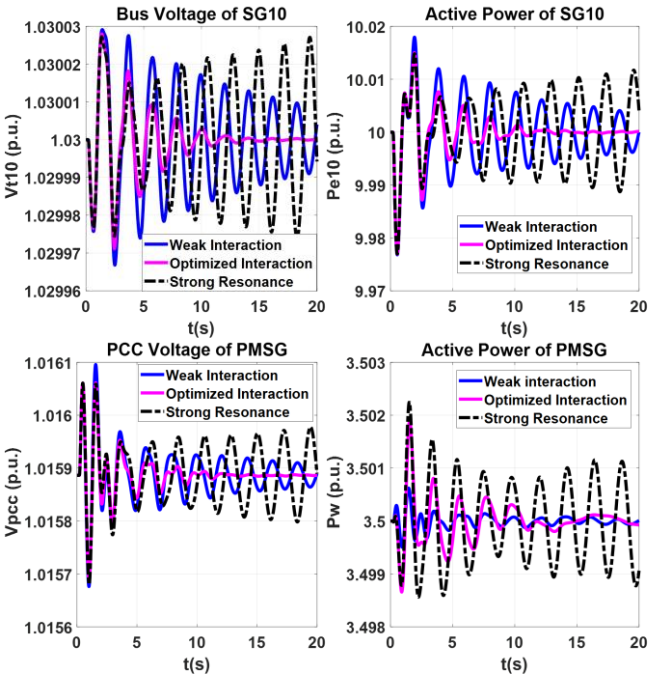

Fig. 17 Small disturbance dynamics comparison: Pw=3.5p.u.

D.2 Large Disturbance Response

The simulation condition is set to be: at t=0.2s, a **three-phase to earth short circuit** occurs at Bus 1 and subsequently clears after 100ms. Three categories of dynamic interactions with different power injections (Pw increases from 1.5 p.u. ~ 3.5 p.u.) are investigated. The terminal bus voltage and active power output of SG10 and PMSG are compared, as shown in Fig. 18~ Fig. 20.

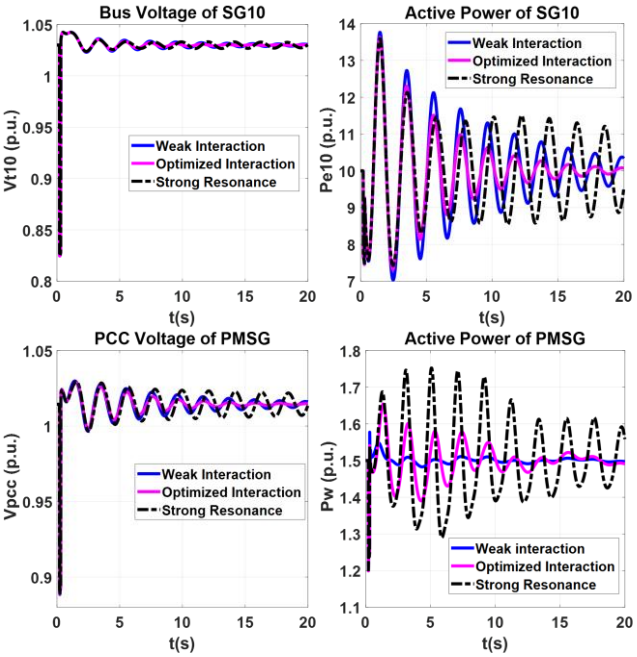

Fig. 18 Large disturbance dynamics comparison: Pw=1.5p.u.

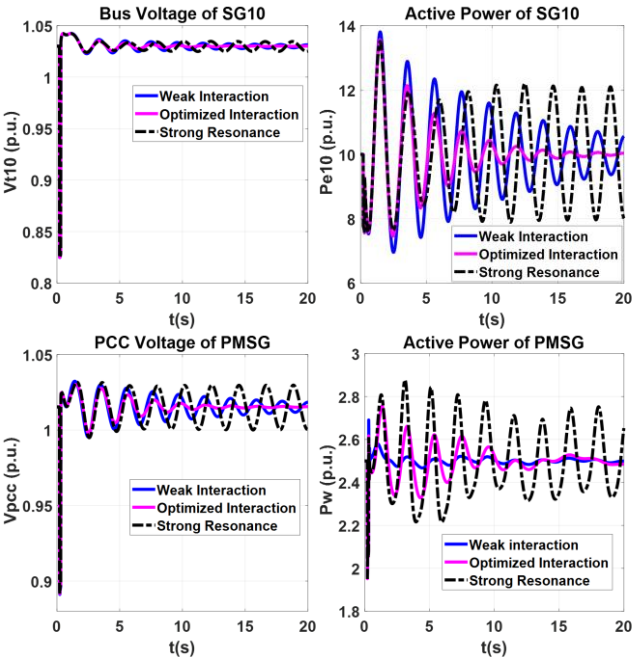

Fig. 19 Large disturbance dynamics comparison: Pw=2.5p.u.

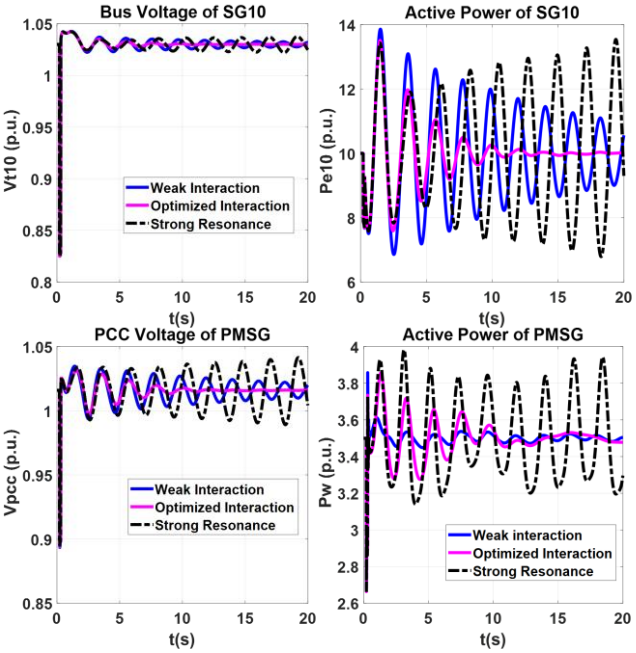

Fig. 20 Large disturbance dynamics comparison: Pw=1.5p.u.

D.3 Discussion on Time Domain Simulations

If the wind power penetration level is low, i.e. the active power output is low, the impact of PMSG on LFO stability is limited. Whereas if the wind power penetration level increases, the impact on MMPS become eminent, oscillation becomes drastic especially when strong resonance happens.

It is also worth mentioning that, with optimized interactions, the LFO of the critical EOM can be effectively damped. With more wind power injection of PMSG into the power system, the ability to damp the LFO also becomes stronger, which means with properly optimized interaction, the integration of FCWG can effectively mitigate the LFO, the positive mitigation can be amplified by the increasing wind

power injection.

Simulation results in both small disturbance and large disturbance have supported that the optimized interactions work effectively especially in weak damping conditions and can significantly maximize the damping ratio of the critical EOM.

E. The Replacement of SG with FCWG

To test the adaptability of the proposed modal coordination strategy, a SG is replaced by FCWG in another different test system (viz., two-area power system), as illustrated in Fig. 21.

In the modified two-area power system, a third-order model of the SGs and a simple first-order model of the AVR are used with no power system stabilizers (PSS) equipped. The loads at Bus 7 and Bus 9 are modeled as constant impedance. The detailed model and parameters of the power system are given in [23]. The detailed 15th-order FCWG is used to replace SG1 with the same power output. FCWG adopts the reactive power control with constant power factor. The power load flow change is balance by G3 at slack Bus 3.

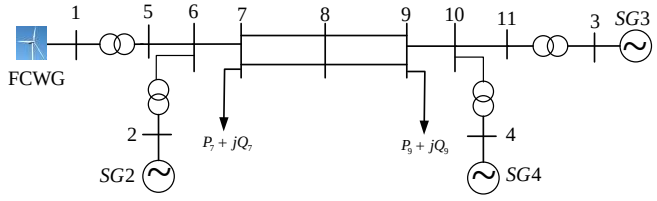

Fig. 21 Configuration of modified two-area power system integrated with an FCWG wind farm.

The same analysis process is implemented in this two-area system. Due to space limit, only the modal analyses and time domain simulation results are briefly discussed.

With typical control parameters, the critical EOM is calculated to be -0.1218 + 3.7919i (damping ratio=**3.21%**) via modal analysis. If the parameters are not properly tuned, for example, the strong resonance happens, and then critical EOM is forced to move to -0.0099 + 3.6500i with a very low damping ratio of **0.27%**. However, after performing the optimal modal coordination, the critical EOM is relocated to -0.2985 + 3.6371i with a high damping ratio of **8.18%**.

The small disturbance condition is set to be: at t=0.2s, a **5% step increase of mechanical power reference** occurs at SG2 and subsequently drops to original after 100ms. The large disturbance condition is set to be: at t=0.2s, a **three-phase to earth short circuit** occurs at Bus 2 and subsequently clears after 100ms. Due to the limitation of space, only the terminal bus voltage and active power output of SG3 and PMSG are compared as shown in Fig. 22 and Fig. 23.

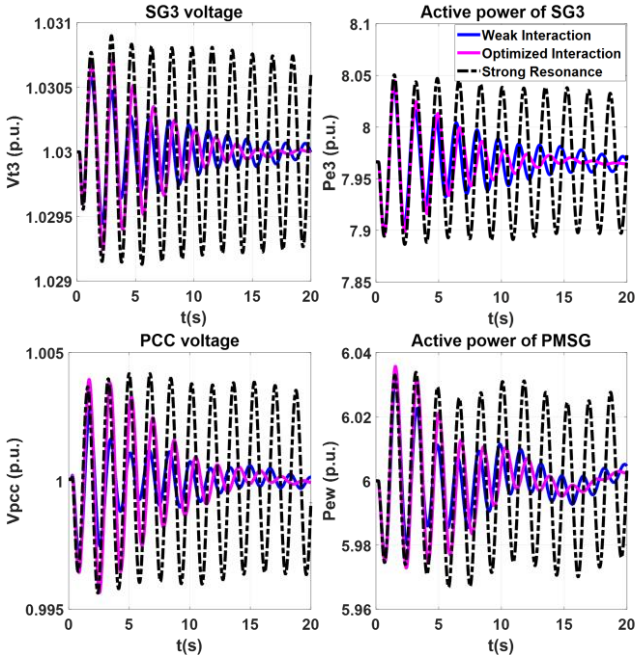

Fig. 22 Small disturbance dynamics comparison in two-area system.

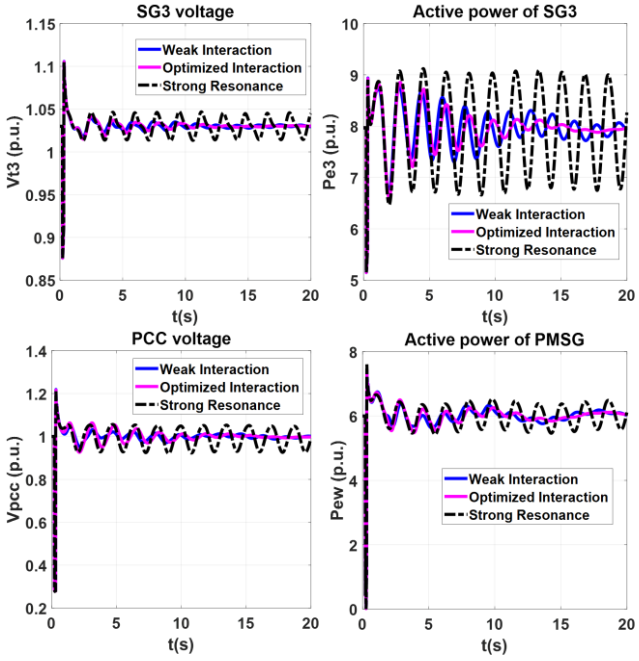

Fig. 23 Large disturbance dynamics comparison in two-area system.

Same findings can be concluded. Improper tuning of controller parameters in FCWG may induce negative impact on LFO stability. With optimal modal coordination strategy, it is possible to impose beneficial dynamic interactions. As a result, the system damping is greatly enhanced as well as the LFO stability.

VI. Conclusion

An optimal modal coordination strategy to mitigate low frequency oscillation in FCWG penetrated power systems has been proposed in this paper. The significant findings are exhibited as follows.

i) Modal superposition theory analyzes the all the possibilities of modal interactions between FCWG and MMPS. One of the modal interactions (viz. modal counteraction) is proved to be effective in improving system damping.

ii) Three categories of modal coupling are visualized in the complex plane. Modal coupling mechanism is investigated to support the important finding that modal counteraction can significantly suppress LFOs in a weak damping MMPS especially.

iii) An optimal modal coordination strategy is proposed to relocate FOM to induce modal counteraction with the critical EOM of MMPS. Satisfactory damping performance are attained after optimization with different operation points.

iv) Time domain simulation results also validate the superior damping effect and effectiveness of the optimized modal interaction over the normal weak interaction with typical controller parameters in FCWG.

VII. Acknowledgment

The authors would like to acknowledge the support from National Natural Science Foundation of China for the Research Project (51807171), Guangdong Science and Technology Department for the Research Project (2019A1515011226), Hong Kong Research Grant Council for the Research Projects (25203917), (15200418) and (15219619), and Department of Electrical Engineering, The Hong Kong Polytechnic University for the Start-up Fund Research Project (1-ZE68).

References

[1] J. Morato, T. Knuppel, and J. Ostergaard, "Residue-Based Evaluation of the Use of Wind Power Plants With Full Converter Wind Turbines for Power Oscillation Damping Control," IEEE Transactions on Sustainable Energy, vol. 5, no. 1, pp. 82-89, 2014.

[2] M. Hedayati-Mehdiabadi, J. Zhang, and K. W. Hedman, "Wind Power Dispatch Margin for Flexible Energy and Reserve Scheduling With Increased Wind Generation," IEEE Transactions on Sustainable Energy, vol. 6, no. 4, pp. 1543-1552, 2015.

[3] N. Nguyen and J. Mitra, "Reliability of Power System with High Wind Penetration Under Frequency Stability Constraint," IEEE Transactions on Power Systems, vol. 33, no. 1, pp. 985-994, 2018.

[4] J. Sun et al., "Renewable energy transmission by HVDC across the continent: system challenges and opportunities," CSEE Journal of Power and Energy Systems, vol. 3, no. 4, pp. 353-364, 2017.

[5] G. Li, G. Li, and M. Zhou, "Model and application of renewable energy accommodation capacity calculation considering utilization level of inter-provincial tie-line," Protection and Control of Modern Power Systems, vol. 4, no. 1, pp. 1-12, 2019.

[6] H. Li and Z. Chen, "Overview of different wind generator systems and their comparisons," IET Renewable Power Generation, vol. 2, no. 2, pp. 123-138, 2008.

[7] W. Zhang, D. Remon, I. Candela, A. Luna, and P. Rodriguez, "Grid-connected converters with virtual electromechanical characteristics: experimental verification," CSEE Journal of Power and Energy Systems, vol. 3, no. 3, pp. 286-295, 2017.

[8] S. Boubzizi, H. Abid, and M. Chaabane, "Comparative study of three types of controllers for DFIG in wind energy conversion system," Protection and Control of Modern Power Systems, vol. 3, no. 1, pp. 21-32, 2018.

[9] W. Du, J. Bi, J. Cao, and H. F. Wang, "A Method to Examine the Impact of Grid Connection of the DFIGs on Power System Electromechanical Oscillation Modes," IEEE Transactions on Power Systems, vol. 31, no. 5, pp. 3775-3784, 2016.

[10] Y. Li, Z. Xu, and K. P. Wong, "Advanced Control Strategies of PMSG-Based Wind Turbines for System Inertia Support," IEEE Transactions on Power Systems, vol. 32, no. 4, pp. 3027-3037, 2017.

[11] Y. Wang, J. Meng, X. Zhang, and L. Xu, "Control of PMSG-Based Wind Turbines for System Inertial Response and Power Oscillation Damping," IEEE Transactions on Sustainable Energy, vol. 6, no. 2, pp. 565-574, 2015.

[12] J. Xi, H. Geng, G. Yang, and S. Ma, "Inertial response analysis of PMSG-based WECS with VSG control," The Journal of Engineering, vol. 2017, no. 13, pp. 897-901, 2017.

[13] J. Licari and J. Ekanayake, "Coordinated inertia response from permanent magnet synchronous generator (PMSG) based wind farms," Journal of the National Science Foundation of Sri Lanka, vol. 43, no. 4, pp. 347-355, 2015.

[14] L. M. Fernández, F. Jurado, and J. R. Saenz, "Aggregated dynamic model for wind farms with doubly fed induction generator wind turbines," Renewable energy, vol. 33, no. 1, pp. 129-140, 2008.

[15] J. T. Bialasiewicz and E. Muljadi, "The wind farm aggregation impact on power quality," in IECON 2006-32nd Annual Conference on IEEE Industrial Electronics, 2006, pp. 4195-4200.

[16] R. Piwko, N. Miller, J. Sanchez-Gasca, X. Yuan, R. Dai, and J. Lyons, "Integrating large wind farms into weak power grids with long transmission lines," in 2006 CES/IEEE 5th International Power Electronics and Motion Control Conference, 2006, vol. 2, pp. 1-7.

[17] S. Li, T. A. Haskew, R. P. Swatloski, and W. J. I. T. o. p. e. Gathings, "Optimal and direct-current vector control of direct-driven PMSG wind turbines," vol. 27, no. 5, pp. 2325-2337, 2011.

[18] W. Du, X. Chen, and H. F. Wang, "Power System Electromechanical Oscillation Modes as Affected by Dynamic Interactions From Grid-Connected PMSGs for Wind Power Generation," IEEE Transactions on Sustainable Energy, vol. 8, no. 3, pp. 1301-1312, 2017.

[19] X.-F. Wang, Y. Song, and M. Irving, Modern power systems analysis. Springer Science & Business Media, 2010.

[20] J. Rocabert, A. Luna, F. Blaabjerg, and P. Rodriguez, "Control of power converters in AC microgrids," IEEE transactions on power electronics, vol. 27, no. 11, pp. 4734-4749, 2012.

[21] S. Bu, W. Du, and H. Wang, "Model validation of DFIGs for power system oscillation stability analysis," IET Renewable Power Generation, vol. 11, no. 6, pp. 858-866, 2017.

[22] S. Bu, X. Zhang, J. Zhu, and X. Liu, "Comparison analysis on damping mechanisms of power systems with induction generator based wind power generation," International Journal of Electrical Power & Energy Systems, vol. 97, pp. 250-261, 2018.

[23] P. Kundur, N. J. Balu, and M. G. Lauby, Power system stability and control. McGraw-hill New York, 1994.

[24] H.-W. Kim, S.-S. Kim, and H.-S. Ko, "Modeling and control of PMSG-based variable-speed wind turbine," Electric Power Systems Research, vol. 80, no. 1, pp. 46-52, 2010.

[25] W. Du, J. Bi, and H. Wang, "Damping Degradation of Power System Low-Frequency Electromechanical Oscillations Caused by Open-Loop Modal Resonance," IEEE Transactions on Power Systems, vol. 33, no. 5, pp. 5072-5081, 2018.

[26] Singular values plot of dynamic system. Available: https://nl.mathworks.com/help/control/ref/sigma.html